### **REVIEW**



# Orientational Selectivity in Pulsed-EPR Does Not Have to be Complicated

Zikri Hasanbasri<sup>1</sup> · Sunil Saxena<sup>1</sup>

Received: 14 July 2023 / Revised: 1 August 2023 / Accepted: 4 August 2023 © The Author(s), under exclusive licence to Springer-Verlag GmbH Austria, part of Springer Nature 2023

## **Abstract**

The development of rigid spin labels and high-frequency spectrometers have improved the capabilities of pulsed-EPR distance measurements in the field of structural biology. Rigid spin labels provide distance constraints that better report on the conformations of the protein or DNA backbone. Additionally, spectrometers at high frequencies improve the sensitivity of pulsed-EPR, even enabling experiments at concentrations close to cellular conditions. Unfortunately, these advents can come with a complication in that the microwave pulse cannot completely sample all orientations of the spins. Consequently, insufficient sampling biases the dipolar frequencies in a manner that depends on the relative orientations of the intramolecularly interacting spins. These relative orientations are generally unknown a priori in a bilabeled biomolecule. This biasing effect, dubbed 'orientational selectivity,' is a bottleneck to interpreting distance measurements from the dipolar signal. This review provides an overview of orientational selectivity in the context of distance measurements using Double Electron-Electron Resonance. First, we discuss the genesis of orientational selectivity and briefly overview the literature on spin labels that have manifested orientational selectivity. Second, we outline the various strategies to account for orientational selectivity effects for extracting the distance constraints. Finally, we showcase a new perspective on analyzing orientational selectivity and designing efficient experimental schemes for overcoming orientational selectivity.

## 1 Introduction

In the past three decades, measurements of electron–electron dipolar interactions using pulsed-EPR spectroscopy have been widely adopted since its first inception in 1984 [1]. At first, the measurement of the dipolar interaction between electrons

Published online: 13 August 2023

Department of Chemistry, University of Pittsburgh, Pittsburgh, PA 15260, USA



Sunil Saxena sksaxena@pitt.edu

was used to understand the distributions of radicals in solid materials [2]. However, the application spread further into the field of structural biology after the development of a site-specific spin label, MTSSL, which enabled the incorporation of stable spin labels into proteins [3, 4]. When two spin labels are present on the same biomolecule, various pulsed-dipolar spectroscopy (PDS) methods [2, 5-11] were developed to measure sparse distance constraints. Such structural constraints provide incisive atomic-level insights into ligand-binding sites [12–17], induced conformational changes [18-25], and the relative positioning of biomolecules in large oligomeric assemblies [26–29]. PDS is not limited to the size of the biomolecule, which enables measurements of membrane proteins [21, 30-34] and even proteins in cellular environments [35–42]. The success of distance measurements has spurred the further development of PDS in two aspects. First, MTSSL is a flexible spin label, which leads to distance distributions with more than 4-5 Angstrom standard deviations [43]. Such broad distributions create an intrinsic ambiguity in relating the distance to protein structure, conformational dynamics, and flexibility [44, 45]. This limitation has motivated the development of rigid spin labels such as constrained nitroxides and Cu(II) labels [46, 47]. Figure 1a demonstrates the contrast in the range of conformational space between MTSSL [48] and a constrained Cu(II) label, dHis-Cu(II) [49]. The restricted conformations of dHis-Cu(II) provide distance distributions up to fivefold narrower than distributions from MTSSL [50]. Consequently, rigid labels provide distances that better report on the conformations of the biomolecule. Second, PDS using the commonly available X-band (~9.6 GHz) spectrometers suffers from low sensitivity. As a result, there is ongoing research to extend the PDS methodology to high-frequency spectrometers to increase the sensitivity of pulsed-EPR data. Figure 1B shows the Field Swept electron spin echo

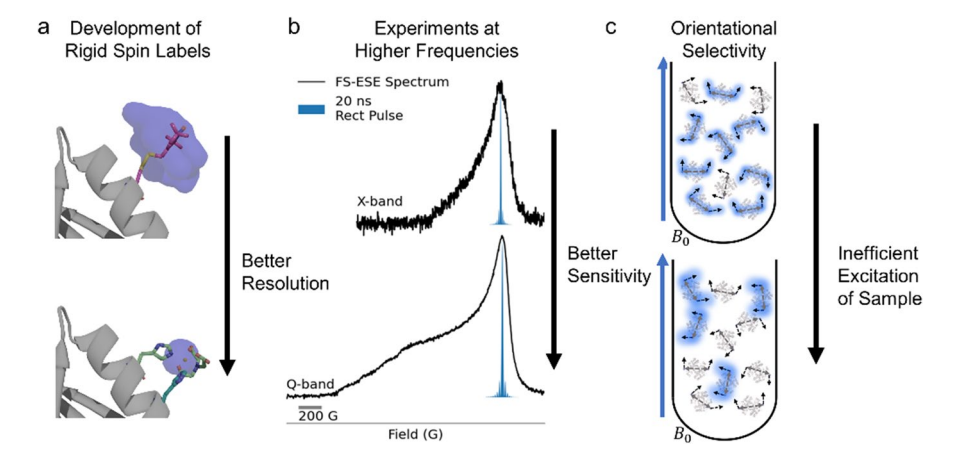


**Fig. 1** a Depiction of the range of conformations for a flexible spin label, MTSSL [48], and a rigid spin label, dHis-Cu(II) [49]. Calculation of R1 conformations is done using ChiLife [59], while the conformations of dHis-Cu(II) are calculated from MD simulations [60]. **b** The Field Swept-Electron Spin Echo spectra of dHis-Cu(II) at X-band and Q-band were collected with the same number of scans. The shaded blue region represents the excitation profile of a 20 ns rectangular pulse. **c** Schematic of how the limited excitation profile pulse can lead to inefficient sample excitation



(FS-ESE) spectrum of dHis-Cu(II) with the same number of scans at X and Q-band (~34 GHz). The improvement in sensitivity at Q-band is evident. Increasing the frequency from X-band to Q-band leads to a ca. 13-fold increase in sensitivity for distance measurements [51]. Consequently, Q-band frequencies have enabled distance measurements at protein concentrations as low as ca. 50–500 nM depending on the spin label [35, 52, 53]. Increasing the frequency further reduces the required sample volume [54–58]. In the next decade, we anticipate more adoption of rigid labels and high-frequency experiments to open new pathways for understanding protein structure and dynamics. However, as we embrace these improvements, the effects of limitations of microwave pulses on PDS measurements are also expected to become more prevalent.

At higher fields, the spectrum bandwidth naturally increases while the bandwidth of pulses remains the same. Figure 1b shows the dHis-Cu(II) spectra at X-band and Q-band. Increasing the frequency from X-band to Q-band leads to a~fourfold increase in spectral breadth. As a result, the pulse excites a smaller fraction of the spins in the sample at Q-band than at X-band. Figure 1c depicts how the number of excited spins, highlighted in blue, decreases with increasing frequency. More importantly, at higher frequencies, the excited spins are more biased to specific orientations of the spins relative to the applied magnetic field. When combined with rigid labels, selective sampling of spin orientations biases the dipolar frequency in a manner unique to the relative orientations of the labels, which is unknown a priori for bilabeled molecules. This effect, dubbed 'orientational selectivity,' convolutes the direct interpretation of the distance constraint from the dipolar frequency. These considerations have spurred the development of shaped pulses [61–64] and loop-gap resonators [65, 66] that improve pulse bandwidth. Given their current state, these new technologies are promising but often cannot eliminate the effects of orientational selectivity, especially for rigid spins with a large g-tensor anisotropy [67].

Measurement of the distance constraint in the presence of orientational selectivity requires one of the two strategies. The first strategy is to sum multiple dipolar signals collected across the spectrum to average the orientational effects [68–73]. The second strategy is to analyze multiple dipolar signals simultaneously to resolve the distance and angular constraints [74–78]. The algorithms for analyzing orientational selectivity use a generalizable analytical expression to simulate a dipolar signal [79]. However, both approaches contain inherent limitations. For example, the measurements can require up to 17 experiments at different magnetic fields across the spectrum to obtain the proper distance distribution from orientational-selective data [73]. Second, as shown in Fig. 1b, the signal intensity of the Cu(II) spectrum decreases significantly at low magnetic fields. Consequently, experiments at magnetic fields with low *SNR* require longer experimental runtimes, further exacerbating the process. Therefore, developing efficient experimental acquisition schemes requires a new perspective on orientational selectivity.

Recently, we have developed a new approach to conceptualize pulsed EPR data and orientational selectivity. This method takes a bottom-up approach by generating an in-silico ensemble of rigidly attached spin-labeled proteins to examine pulse excitation and replicate an orientational-selective sample [80, 81]. This approach differs from other software since each spin pair is individually interrogated to tabulate the



spin pairs contributing to the dipolar signal under a specific experimental condition. By dissecting the simulated dipolar signal into its components, the in-silico sample approach enables the development of strategies for efficient data acquisition.

This review provides the current state of orientational selectivity in literature, focusing mainly on Double Electron–Electron Resonance (DEER) experiments [2, 6]. We provide this review in three sections. Section one discusses the origin of orientational selectivity, while section two describes the traditional methodology for overcoming orientational selectivity. The last section describes the in-silico sample approach to design efficient experimental acquisition schemes.

## 2 Discussion

# 2.1 The Origin of Orientational Selectivity

The intramolecular DEER equation is given by the following Equation:

$$V_{\text{intra}}(t) = \int_{0^{\circ}}^{90^{\circ}} \lambda \left(1 - \cos\left(\omega_{ee}t\right)\right) P(\theta) P(r) d\theta dr \tag{1}$$

In Eq. 1,  $\lambda$  is the modulation depth of the signal,  $\theta$  is the angle between the applied magnetic field and the interspin vector  $\mathbf{r}$ , and  $\omega_{ee}$  is the angular velocity of the intramolecular magnetic dipolar interaction of the two spins:

$$\omega_{ee} = \frac{\mu_0 g_A g_B \beta_e^2}{4\pi \hbar r^3} (3\cos^2(\theta) - 1)$$
 (2)

where  $\mu_0$  is the vacuum magnetic permeability,  $g_A$  and  $g_B$  are the g-value of Spin A and Spin B,  $\beta_e$  is the Bohr Magneton, and h is the Planck constant. Equation 1 highlights that translating the DEER signal into the distance distribution, P(r), requires knowledge of the distribution of  $\theta$ , i.e.,  $P(\theta)$ , sampled in the experiment. Figure 2a shows a schematic that defines angles  $\phi$  and  $\theta$  in a test tube containing doubly labeled dHis-Cu(II) proteins. The blue arrows represent the direction of the  $g_{\parallel}$ -axis of the two spins, while the dotted black arrows represent the interspin vector, r. The angle between  $B_0$  and r is denoted by  $\theta$  while the angle between  $B_0$  and the  $g_{\parallel}$ -axis of each spin is denoted by  $\phi$ . For distance measurements, all  $\theta$  angles must be sampled, and under this condition,  $P(\theta)$  is simply  $\sin(\theta)$ , which is the statistical distribution of  $\theta$  in a frozen solution or powder sample. This assumption is generally valid for DEER experiments with nitroxide [4], trityl [82], Gd(III) spins [83], or even Cu(II) [84–87] that use flexible linkers.

Figure 2b shows how the relative orientations between the *g*-tensors of the two spins and r can be described with three angular parameters,  $\chi$ ,  $\gamma$ , and  $\eta$ . Three parameters are sufficient for describing spins with axial geometries [75], such as Cu(II) labels. In comparison, five parameters are required for spins with rhombic geometries [88], such as nitroxide labels. Each angular parameter also has its distribution. Figure 2c depicts how the conformations of a label dictate the distributions of  $\chi$ ,  $\gamma$ , and  $\eta$  angles ( $\Delta \chi$ ,  $\Delta \gamma$  and  $\Delta \eta$ ). Spin labels with flexible linkers



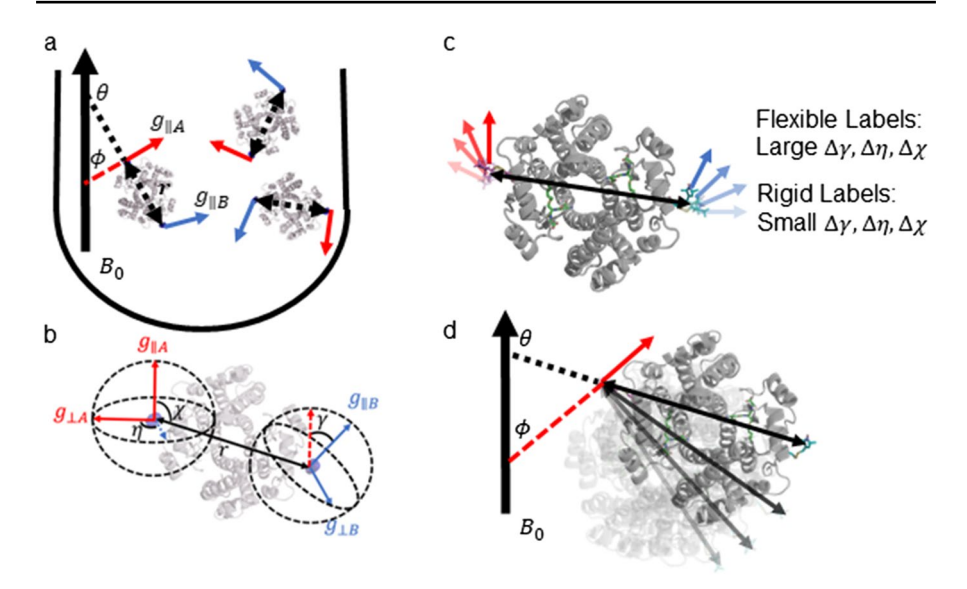


Fig. 2 a Schematic of a test tube containing bilabeled proteins. The blue arrows represent the  $g_{\parallel}$ -axes of each spin and the dashed black arrows represent the interspin vector,  $\mathbf{r}$ . The applied magnetic field,  $B_0$ , is shown as the solid black line. The angles  $\phi$  and  $\theta$  denote the orientations of the  $g_{\parallel}$ -axes of each spin and  $\mathbf{r}$ , respectively, with respect to  $B_0$ .  $\mathbf{b}$  The relative orientations between the axial g-tensors and  $\mathbf{r}$  are described with three angular parameters; the angle between the  $g_{\parallel}$  of Spin A and  $\mathbf{r}$  ( $\chi$ ), the angle between the  $g_{\parallel}$ -axes of Spin A and Spin B ( $\gamma$ ), and the angle between the  $g_{\perp}$ -axes of the two spins ( $\eta$ ).  $\mathbf{c}$  Depiction of the range of  $\chi$ ,  $\gamma$ , and  $\eta$  accessible for either flexible or rigid spin labels.  $\mathbf{d}$  Depiction of the bilabeled proteins with the  $g_{\parallel}$ -axes of Spin A aligned. The range of orientations of accessible  $\theta$  for a given  $\phi$  depends on  $\Delta \chi$ . These figures highlight how large distributions in the relative orientations can minimize orientational selectivity

have large distributions for each angular parameters due to their large degree of freedom. On the other hand, rigidly attached dHis-Cu(II) labels have angular distributions that primarily depend on the elasticity of the coordination environment [60, 89]. These angular distributions determine the extent of orientational selectivity. Figure 2d shows the spin-labeled proteins with the  $g_{\parallel}$ -axes of Spin A aligned. The figure illustrates how large distributions in relative orientations reduce orientational selectivity, using the distribution in  $\chi$  as an example. As is clear from Fig. 2d, flexible spin labels with large  $\Delta \chi$  have a large distribution of  $\theta$  angles for excitation at any given  $\phi$  angle. As a result, achieving  $P(\theta)$  as  $\sin(\theta)$  is easy, even if the sampled  $\phi$  angles are limited. However, this assumption is not valid for rigid labels where  $\Delta \chi$  is small. When a pulse selectively samples  $\phi$ , the range of accessible  $\theta$  is also limited, hence the term 'orientational' selectivity.

The correlative nature between  $\phi$  and  $\theta$  in rigid spin labels can be discussed theoretically and experimentally in the context of dHis-Cu(II) DEER experiments. The spin-label dHis-Cu(II) attaches to a protein by forming coordination between Cu(II) and two histidine residues [50, 90–92]. The dHis-Cu(II) is a useful example because the spin label exhibits orientational selectivity effects



at Q-band frequencies but not at X-band [73, 81, 89]. Therefore, the distance distribution from X-band DEER with dHis-Cu(II) is a useful comparison for testing the interpretation of distances from Q-band data.

We can rationalize the presence and absence of orientational selectivity in Q-band and X-band, respectively, based on the spectra of dHis-Cu(II). Figure 3a shows the FS-ESE spectrum of dHis-Cu(II) at either X-band or Q-band frequency. The spectrum of spins with  $\phi$  angles of 0°, 45°, and 90° are overlaid as red, purple, and blue solid lines, respectively. These resonant fields are easily calculated using the established EPR theory [93] and the measured g and A-tensors of dHis-Cu(II) [94, 95] as inputs. Compared to X-band, the high frequency of Q-band causes the resonant field to separate between the different  $\phi$  angles. More importantly, the large spread of the resonant fields at Q-band is significantly larger than the excitation bandwidth of commercially available pulses. Figure 3a shows the excitation bandwidth of a 20 ns rectangular pulse as the shaded blue region. At X-band, despite the narrow excitation bandwidth, the pulse samples a large range  $\phi$  angles. On the other hand, at Q-band, the range of  $\phi$  angles that are excited by the pulse is limited.

Figure 3b shows  $P(\phi)$  and  $P(\theta)$  sampled by the rectangular pulse as orange and green lines, respectively. The details of calculations of  $P(\theta)$  and  $P(\phi)$  are described in previous publications [80, 81].  $P(\phi)$  is based on the  $\phi$  angles of Cu(II) spins with resonant fields overlapping with the pulse shown in Fig. 3a. On the other hand,  $P(\theta)$  is obtained for a specific relative orientations of  $\chi = 90^{\circ} \pm 10^{\circ}$ ,  $\gamma = 90^{\circ} \pm 10^{\circ}$ , and  $\eta$ 

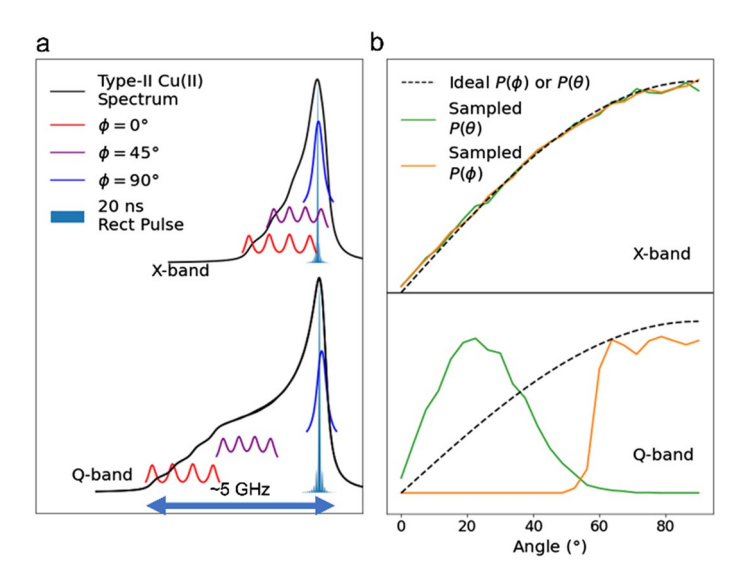


**Fig. 3** a The simulated Field Swept-Electron Spin Echo spectra of dHis-Cu(II) at X-band and Q-band, shown as black lines. The red, purple, and blue curves represent the resonant fields of dHis-Cu(II) spins with  $\phi$  angles of 0°, 45°, and 90°, respectively. The shaded blue line represents the excitation profile of a 20 ns rectangular pulse. **b** The distribution of  $\phi$  and  $\theta$  sampled by the pulse depicted in (**a**). For comparison, the statistical distribution for both  $\phi$  and  $\theta$  are shown as the dashed black line. At X-band, both sampled  $\phi$  and  $\theta$  agree with the statistical distribution. On the other hand, the sampled  $\phi$  and  $\theta$  at Q-band are heavily skewed. The distributions of sampled  $\phi$  and  $\theta$  are calculated based on the relative orientations of  $\chi$ =90°,  $\chi$ =90°, and  $\eta$ =90°



=90 °± 10 ° used in this figure. The relative orientations were chosen to demonstrate the contrast of  $P(\theta)$  between X-band and Q-band. The standard deviations in these angles are conservative estimates based on quantum chemical calculations and MD simulations [46, 60]. For comparison, the dashed black line represents the statistical distribution of  $\phi$  and  $\theta$ . For X-band, because the pulse can sample  $\phi$  angles very well, the sampled  $\theta$  angles match the ideal  $P(\theta)$ . However, for Q-band, the sampled  $\phi$  angles are limited and skewed. Given the narrow  $\Delta \chi$  for rigid spin labels, the sampled  $\theta$  angles are also limited and skewed. Furthermore, the sampled  $\theta$  angles are biased in a manner dependent on the relative orientations of the two spin labels, i.e.,  $\chi$ ,  $\gamma$ , and  $\eta$ , which are unknown for most cases. As a result, orientational selectivity effects are hard to predict for any given bilabeled biomolecule before the experiments.

Additionally, the effects of orientational selectivity vary across the spectrum of the spins. Figure 4a shows the Q-band Cu(II) spectrum where dots mark different magnetic fields. The separation between each dot is 300 MHz, approximately the bandwidth of commercially available resonators. Figure 4b shows the simulated DEER signals color-coded to correspond with the different magnetic fields from Fig. 4a. Details of the simulations are described in previous works [80, 81]. The simulations used the relative orientations where the two  $g_{\parallel}$ -axes of Cu(II) spins on a protein are parallel to each other, depicted in Fig. 4c. Additionally, r is perpendicular to the two  $g_{\parallel}$ -axes. We expect slight fluctuations in the relative orientations of the three vectors due to the fluctuations in the coordination environment of dHis-Cu(II) [60].

Figure 4a and b conceptually demonstrate how sampling different populations of Cu(II) spins leads to differences in the frequencies of the dipolar signal as the magnetic fields change. As per EQ.1, the differences in the DEER signal are due to differences in  $P(\theta)$  across the Cu(II) spectrum. The correlation between the sampled  $P(\phi)$  and  $P(\theta)$  embedded in each DEER signal corresponds to the specific relative orientation of the spin system, which has been demonstrated in various rigid spin labels.

Figure 5 shows the different spin labels that have shown orientational selectivity in DEER experiments. These rigid spin labels were initially developed to measure

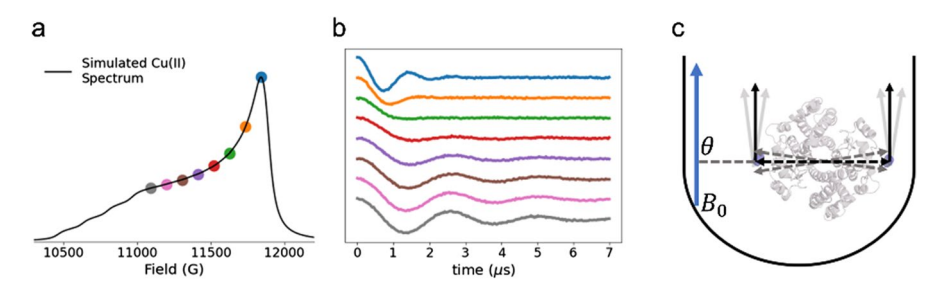


**Fig. 4** a The simulated dHis-Cu(II) FS-ESE spectrum at Q-band. The color-coded dots are separated by 300 MHz, which is the resonator bandwidth of commercially available resonators. **b** Simulations of the DEER signal based on the different magnetic fields denoted by the dots in (a). The simulations were calculated based on  $\chi=90^{\circ}$ ,  $\gamma=0^{\circ}$ , and  $\eta=0^{\circ}$ , which are depicted in (c)



	Protein Labels	DNA/RNA Labels
Nitroxide	TOPP	o' Ç
	H <sub>2</sub> N N-O	NH NN N
	RX	<b>G</b>
	Protein N-O	HN-H-N-N-N-N-N-N-N-N-N-N-N-N-N-N-N-N-N-
Copper	dHis-Cu(II)	Cu(II)-G-Quadruplex
	Protein N N N N N N N N N N N N N N N N N N N	Oligonucleotide Oligonucleotide Oligonucleotide Oligonucleotide

Fig. 5 Lewis structures of different rigid nitroxide (TOPP [96], RX [98], C [105], and C [107]) and Cu(II) (dHis-Cu [50] and Cu(II)-G-Quadruplex [110]) labels that have demonstrated orientational selectivity

distances that closely resemble the constraints of the protein backbone. For example, TOPP is a semi-rigid nitroxide label that labels directly on the peptide bond of the site [96]. Distance measurements using TOPP provided constraints that best represent the length of transmembrane peptides in various lipids [97]. Restraining the nitroxide radical was also achieved with the bifunctional nitroxide RX [98]. Attaching RX to two nearby cysteine residues limits the conformations of the label, providing distance distributions that are more correlative to the protein backbone [98,



99]. Beyond nitroxides, Cu(II)-based rigid labels are also available [46]. Figure 5 shows the labeling scheme for dHis-Cu(II). The rigid dHis-Cu(II) is more poised to resolve small-scale conformational changes [100]. Furthermore, both RX and dHis-Cu(II) can provide relative orientations of secondary structures of the labeled sites based on the orientational selectivity effects [73, 99]. Analysis of the angular constraints can also provide the angle of the transmembrane peptide relative to the membrane [101]. Note that orientational selectivity can manifest with flexible labels if the local environment of the label significantly restricts the conformations of the label [102–104].

Orientational selectivity has also been observed in oligonucleotides using rigid DNA/RNA labels. The spin-label Ç is a cytidine analog with a nitroxide radical that can base-pair to a guanidine in a DNA or RNA [105]. In addition to Ç, non-covalent DNA spin labels, Ġ, were also developed to label DNA at an abasic site [106, 107]. DNA labeling using Cu(II) is also available with Cu(II)-G-Quadruplex [108–110]. These rigid spin labels can resolve the dynamical modes of motion of the DNA backbone [70, 111]. Furthermore, rigid DNA labels enabled measurement of the tilting angle of the ends of the DNA [108]. The angular constraints also shed light on the bending and twisting of the DNA upon a protein or ligand-induced conformational change [68, 112]. These examples highlight how orientational selectivity is rich with structural information. Translating the DEER signal into these structural constraints requires algorithms and software to analyze the orientational selectivity effects and output the correct distance and relative orientations.

# 2.2 Traditional Methodology for Overcoming Orientational Selectivity

Most algorithms for understanding orientational selectivity fall under a model-based approach, where the relative orientations of the spin pairs are used as part of the inputs to simulate the dipolar signal [74–78, 113, 114]. Figure 6 shows a general schematic of a model-based approach. Figure 6a shows how the angular parameters,  $\chi$ ,  $\gamma$ , and  $\eta$  and their distribution widths can be used as inputs to build a model of the spin-labeled proteins. Note that for nitroxides five angles are needed. The generated models can provide a simulated DEER signal, which is then numerically compared with the experimental DEER signal, as shown in Fig. 6b. The model-based approach generally relies on reiteratively varying the inputs to refine the initial model and find the minimal RMSD between the simulated and experimental DEER signal. These model-based algorithms have been developed to resolve the angular constraints in model biradicals [76, 88, 115–117] and biomolecules [74, 75, 99, 104, 118–120]. Note that an orientational selective dipolar signal can have multiple solutions for the angular constraints due to the symmetry of the g-tensors [77].

Alternatives to the model-based algorithms are also available for overcoming orientational selectivity. Recently, a new analytical approach based on spherical harmonics [78] described DEER spectra as a linear combination of 'modified' Pake Patterns (MPP). This description of the DEER spectra allows for P(r) to be extracted from the MPP components while the orientational selectivity effects are embedded in the weights of each MPP component. This approach requires only minutes



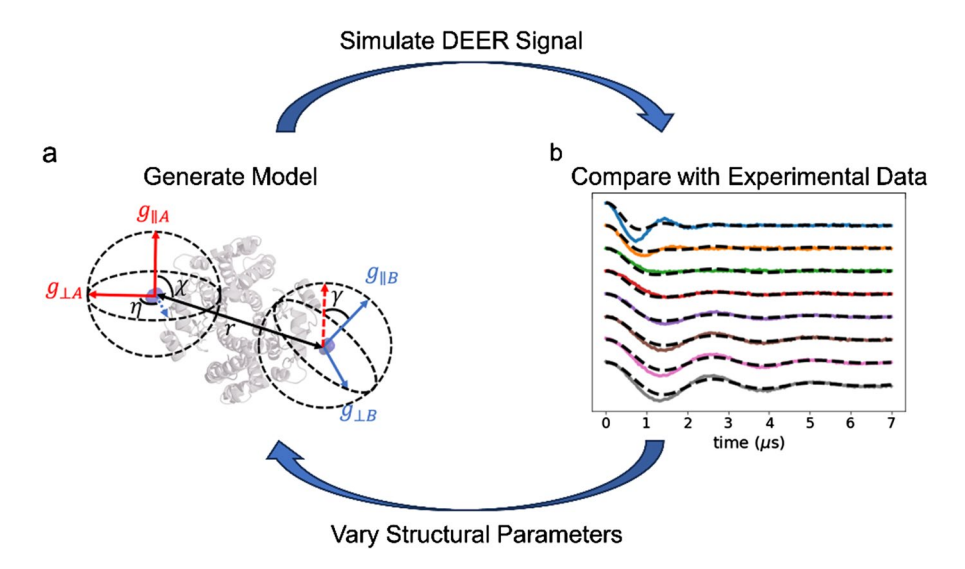


Fig. 6 Schematic of the general procedure of a model-based approach used to analyze orientational-selective data. The procedure starts with  $(\mathbf{a})$ , where a model of the spin-labeled protein is generated using an initial input of the relative orientations. The model then allows for the simulation of the DEER signal, which is then numerically compared with the experimental data in  $(\mathbf{b})$ . The RMSD of the comparison is optimized by reiteratively adjusting the relative orientations of the model. Sufficient agreement between the simulation and the experimental data enables the extraction of the relative orientations and r from the fitted model

of computational time using a regular desktop PC. However, the approach currently cannot provide an obvious interpretation of the angular constraints solely from the weights of the MPP components. In addition to these algorithms, orientational selectivity effects can be averaged out by summing the different DEER signals across the spectrum of the spins [121], enabling direct interpretation of distances using Tikhonov regularization [122]. The solved P(r) can then be inputted into the model for fitting of the angular parameters if the angular constraints are still of interest.

Across these algorithms and strategies, multiple DEER experiments are a prerequisite for extracting distance constraints. However, a question remains: what is the most efficient way to obtain distance constraints with the least DEER experiments? In theory, the solution is to identify the smallest number of experiments required for a sufficient sampling of the molecular orientations in the sample. Specifically, the DEER experiments must be designed to sample  $P(\theta)$ =sin( $\theta$ ), as per EQ.1. Unfortunately, current analytical and numerical approximations of orientational selectivity cannot easily provide information of  $P(\theta)$ .

## 2.3 The In-Silico Approach for Designing Efficient Acquisition Schemes

We have recently developed an in-silico sample approach to optimize the acquisition scheme for dHis-Cu(II) [80, 81]. The scheme follows the philosophy that sampling  $P(\theta)=\sin(\theta)$  in the sample is achievable as long as the DEER experiments



sufficiently sample the  $\phi$  angles. Shifting the focus to  $\phi$  angles is beneficial since information of  $\phi$  only depends on the g and A-tensors of the spin label and not on relative orientation. The values of the g and A-tensors can be easily measured for the spin label using continuous wave EPR measurements at low temperatures. Therefore, designing acquisition schemes that enhance the sampling of  $\phi$  angles naturally optimizes the sampling of  $\theta$ , without the need for knowledge of the relative orientations of the spins.

Figure 7 shows the general workflow of the recently developed in-silico sample approach. In the first step, consider an ensemble of randomly oriented bilabeled proteins. The relative orientations of each bilabeled protein are sampled from the distributions of angular parameters  $(\chi, \gamma, \eta, \Delta \chi, \Delta \gamma, \Delta \eta)$  set by the user. Note that the choice of angular parameters is only to initiate the workflow, and testing of all relative orientations is considered later in the workflow. The resonant fields for each spin can be easily calculated [93]. Step 1 shows the spectra of different spins, color-coded based on the  $\phi$  angles. The spectrum from each spin enables the tabulation and quantification of the number of  $\phi$  angles at each magnetic field in the spectrum. The quantification of  $\phi$  is represented as the blue curve, labeled as the  $\Phi$ -curve. Details of the  $\Phi$ -curve calculations are provided in previous works [80, 81]. The  $\Phi$ -curve maximum represents the magnetic field where a pulse can sample the greatest number of  $\phi$  angles. Therefore, this magnetic field is the most promising position for pumping the greatest number of  $\theta$  angles.

The next step is to simulate the DEER experiment with the pump pulse placed at this magnetic field. Step 2 shows a schematic of a DEER experiment where the pump and observer pulses are depicted as the shaded green and blue regions, respectively. Given that the resonant fields of each spin are known, the green and blue circles mark the spins excited by either the pump or observer pulses, respectively. Only the spin pairs with both excited spins contribute toward the intramolecular DEER signal. Once identified, the sampled  $\theta$  angles from each excited spin pair are tabulated to form the overall  $P(\theta)$  from the particular DEER experiment in Step 3. Details of pulse implementation are provided in previous works [80, 81]. The sampled  $\theta$  angles are then assessed to ascertain whether  $P(\theta) = \sin(\theta)$ .

If  $P(\theta) \neq \sin(\theta)$ , additional DEER experiments are required to fulfill the gap between  $P(\theta)$  from the previous DEER and the ideal  $\sin(\theta)$ . We hypothesized that the next DEER should focus on the spin pairs in the ensemble that are not excited yet. Therefore, in Step 4, the excited spin pairs from the first DEER are removed. This new ensemble of spin pairs is then used to recalculate a new  $\Phi$ -curve in Step 5. The new  $\Phi$ -curve maximum is then used for the position of the next DEER simulation in Step 2. The cycle from Step 2 to Step 5 reiterates until the summed  $P(\theta)$  from the different DEER simulations matches with  $\sin(\theta)$ , suggesting sufficient sampling of  $\theta$  in the ensemble of bilabeled proteins. The magnetic fields are then recorded after fulfilling the  $\sin(\theta)$  criterion. Finally, the final magnetic fields are tested on all possible relative orientations to ensure that the magnetic fields are universal solutions to all samples labeled by the spin label of interest.

Pleasingly, the workflow outlined in Fig. 7 led to a generalized acquisition scheme for dHis-Cu(II) label at Q-band for 36 ns (or smaller) rectangular pulses that are easily available on commercial spectrometers. If the bandwidth of the resonator



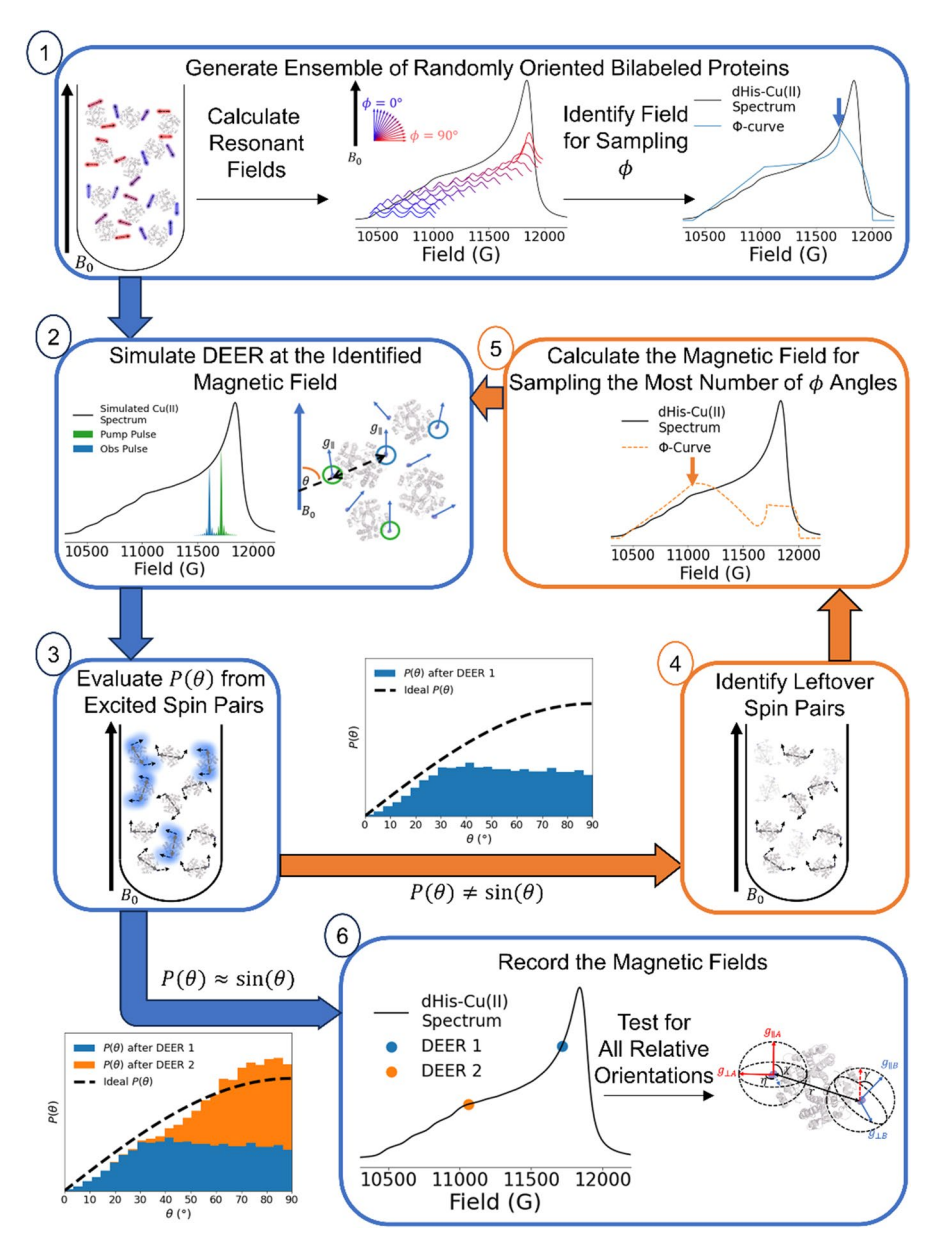


Fig. 7 General workflow of the in-silico sample approach to design efficient acquisition schemes for orientational-independent DEER measurements

enables a resonance offset of 300 MHz or higher, only two DEER acquisitions are needed for orientational-averaged distance measurements [80]. The DEER signals should be obtained with the pump pulses at 127 G and 803 G lower than the maximum of the dHis-Cu(II) spectrum. On the other hand, a frequency offset less than



300 MHz requires three DEERs where the pump pulses are set at 100 G, 580 G, and 827 G lower than the maximum of the dHis-Cu(II) spectrum instead [80, 81]. However, if a minor peak is observed in the distribution, an additional DEER experiment can easily identify if the minor distribution is due to residual orientational selectivity or a minor conformation of the sample [80, 81]. The workflow in Fig. 7 can be easily adapted to design acquisition schemes for different pulse shape [80].

Furthermore, any rigid spin labels can be incorporated by simply altering the g and A-tensors and the appropriate distributions of the relative orientations. Overall, the in-silico sample approach enables designing acquisition schemes for various contexts with the added ability to dissect different factors of orientational selectivity.

The prediction from the in-silico sample was experimentally validated for two different protein samples [80, 81]. Figure 8 shows the distance measurements for the immunoglobulin binding domain of protein G (GB1) and human glutathione-S transferase (hGSTA1-1) in the middle and right panels, respectively. The Q-band distribution was obtained by summing the DEER signals at the two positions depicted by the blue and orange dots in the left panel. The distance distribution from X-band validated the orientational-averaged distance distribution from Q-band. The prominent peaks for GB1 and hGSTA1-1 were also recapitulated from MD simulations [60, 81], supporting the main distributions to be the expected distance. Furthermore, the distributions are also consistent even after summing over ten magnetic

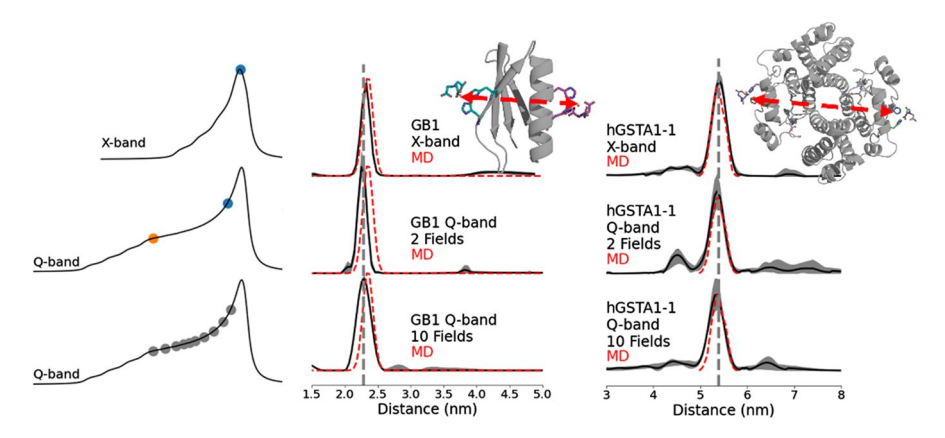


Fig. 8 Experimental distance distributions of dHis-Cu(II) on GB1 and hGSTA1-1 at X-band and Q-band. X-band DEER was performed at the maximum of the dHis-Cu(II) spectrum, denoted by the blue dot. On the other hand, Q-band DEER was performed in two ways. The first Q-band DEER acquisition was performed at two different positions, denoted by the blue and orange dots, while the second acquisition was at ten different fields, denoted by the gray dots. The sum of the DEER signals was analyzed using Tikhonov Regularization [122]. The middle and right panels show the extracted distance distributions as black lines, while the shaded gray corresponds to the error. The dashed red lines represent the distance distribution extracted from MD simulations using the established force-field parameters for dHis-Cu(II) [60]. For both proteins, the orientational-averaged Q-band distance distributions agree with the distribution from the X-band that is known to have minimal orientational selectivity. Furthermore, the Q-band distributions from the two-field acquisition do not change after additional experiments with the ten-field acquisition. These experimental data validate the efficient acquisition of orientational-independent distance measurements at Q-band for dHis-Cu(II), as the in-silico sample approach predicted. Reproduced from Ref. [80, 81] with permission from the PCCP Owner Societies



fields at Q-band [73, 81], further highlighting convergence after two DEERs. Overall, orientational selectivity effects in Q-band were sufficiently averaged with two DEER experiments, as predicted by the in-silico sample approach. More importantly, straightforward extraction of distance constraints of a rigidly attached Cu(II) spin label is achievable without requiring many experiments.

# 3 Concluding Remarks

As the technology for high-frequency EPR spectroscopy develops further, we can expect orientational selectivity to become more prevalent, especially in the field of metalloenzymes, where most paramagnetic metals have large anisotropies. Orientational selectivity will also apply to traditionally non-orientational selective labels, such as trityl if the frequency is high enough to resolve the *g* and *A*-tensors [55]. Furthermore, while this review focuses on DEER experiments, orientational selectivity has also been observed for other distance measurement experiments, such as RIDME [123–125]. Therefore, the fundamentals and the new methodology in this review can easily be adapted for the other PDS techniques. The approach also applies to techniques that measure the interactions between electrons and nuclei [126–132]. Expanding our understanding of orientational selectivity is crucial, whether to ensure we can take advantage of new technologies or unleash more potential from currently available ones.

**Author Contributions** ZH: writing—original draft, writing—review and editing, visualization. SS: writing—review and editing, supervision.

**Funding** This review was financially supported by National Science Foundation [NSF BSF MCB-2006154].

**Availability of Data and Materials** The authors confirm that the datasets generated during and/or analysed during the current study are available from the corresponding author on reasonable request.

### **Declarations**

**Competing interests** The authors have no competing interests.

**Ethical Approval** This research did not contain any studies involving animal or human participants, nor did it take place in any private or protected areas. No specific permissions were required for corresponding locations.

### References

- 1. A.D. Milov, A.B. Ponomarev, Y.D. Tsvetkov, Chem. Phys. Lett. 110, 67 (1984)
- 2. A.D. Milov, A.G. Maryasov, Y.D. Tsvetkov, Appl Magn Reson 15, 107 (1998)
- 3. C. Altenbach, T. Marti, H.G. Khorana, W.L. Hubbell, Science 248, 1088 (1990)
- 4. W.L. Hubbell, C.J. López, C. Altenbach, Z. Yang, Curr. Opin. Struct. Biol. 23, 725 (2013)



- S. Milikisyants, F. Scarpelli, M.G. Finiguerra, M. Ubbink, M. Huber, J. Magn. Reson. 201, 48 (2009)
- 6. M. Pannier, S. Veit, A. Godt, G. Jeschke, H.W. Spiess, J. Magn. Reson. 142, 331 (2000)
- 7. P.P. Borbat, J.H. Freed, Chem. Phys. Lett. **313**, 145 (1999)
- 8. L.V. Kulik, S.A. Dzuba, I.A. Grigoryev, Y.D. Tsvetkov, Chem. Phys. Lett. 343, 315 (2001)
- 9. G. Jeschke, M. Pannier, A. Godt, H.W. Spiess, Chem. Phys. Lett. 331, 243 (2000)
- 10. S. Pribitzer, M. Sajid, M. Hülsmann, A. Godt, G. Jeschke, J. Magn. Reson. 282, 119 (2017)
- 11. M. Bonora, J. Becker, S. Saxena, J. Magn. Reson. **170**, 278 (2004)
- 12. A.K. Upadhyay, P.P. Borbat, J. Wang, J.H. Freed, D.E. Edmondson, Biochemistry 47, 1554 (2008)
- 13. A. Gamble Jarvi, T.F. Cunningham, S. Saxena, Phys. Chem. Chem. Phys. 21, 10238 (2019)
- 14. D. Abdullin, N. Florin, G. Hagelueken, O. Schiemann, Angew. Chem. Int. Ed. 54, 1827 (2015)
- B.J. Gaffney, M.D. Bradshaw, S.D. Frausto, F. Wu, J.H. Freed, P. Borbat, Biophys. J. 103, 2134 (2012)
- D.M. Yin, J.S. Hannam, A. Schmitz, O. Schiemann, G. Hagelueken, M. Famulok, Angew. Chem. Int. Ed. 56, 8417 (2017)
- D. Nguyen, D. Abdullin, C.A. Heubach, T. Pfaffeneder, A. Nguyen, A. Heine, K. Reuter, F. Diederich, O. Schiemann, G. Klebe, Angew. Chem. Int. Ed. 60, 23419 (2021)
- 18. T.E. Assafa, K. Anders, U. Linne, L.-O. Essen, E. Bordignon, Structure 26, 1534 (2018)
- Z. Liu, T.M. Casey, M.E. Blackburn, X. Huang, L. Pham, I.M.S. de Vera, J.D. Carter, J.L. Kear-Scott, A.M. Veloro, L. Galiano, G.E. Fanucci, Phys. Chem. Chem. Phys. 18, 5819 (2016)
- I. Hänelt, D. Wunnicke, E. Bordignon, H.-J. Steinhoff, D.J. Slotboom, Nat. Struct. Mol. Biol. 20, 210 (2013)
- 21. O. Dalmas, P. Sompornpisut, F. Bezanilla, E. Perozo, Nat. Commun. 5, 3590 (2014)
- B. Verhalen, R. Dastvan, S. Thangapandian, Y. Peskova, H.A. Koteiche, R.K. Nakamoto, E. Tajk-horshid, H.S. Mchaourab, Nature 543, 738 (2017)
- 23. B. Joseph, A. Sikora, D.S. Cafiso, J. Am. Chem. Soc. 138, 1844 (2016)
- K. Stone, J. Townsend, J. Sarver, P. Sapienza, S. Saxena, L. Jen-Jacobson, Angew. Chem. Int. Ed. 120, 10346 (2008)
- T. Hett, T. Zbik, S. Mukherjee, H. Matsuoka, W. Bönigk, D. Klose, C. Rouillon, N. Brenner, S. Peuker, R. Klement, H.-J. Steinhoff, H. Grubmüller, R. Seifert, O. Schiemann, U.B. Kaupp, J. Am. Chem. Soc. 143, 6981 (2021)
- S. Milikisiyants, S. Wang, R.A. Munro, M. Donohue, M.E. Ward, D. Bolton, L.S. Brown, T.I. Smirnova, V. Ladizhansky, A.I. Smirnov, J. Mol. Biol. 429, 1903 (2017)
- S.-Y. Park, P.P. Borbat, G. Gonzalez-Bonet, J. Bhatnagar, A.M. Pollard, J.H. Freed, A.M. Bilwes, B.R. Crane, Nat. Struct. Mol. Biol. 13, 400 (2006)
- S. Valera, K. Ackermann, C. Pliotas, H. Huang, J.H. Naismith, B.E. Bode, Chem. Eur. J 22, 4700 (2016)
- H.A. DeBerg, J.R. Bankston, J.C. Rosenbaum, P.S. Brzovic, W.N. Zagotta, S. Stoll, Structure 23, 734 (2015)
- G.E. Fanucci, K.A. Coggshall, N. Cadieux, M. Kim, R.J. Kadner, D.S. Cafiso, Biochemistry 42, 1391 (2003)
- S. Ketter, A. Gopinath, O. Rogozhnikova, D. Trukhin, V.M. Tormyshev, E.G. Bagryanskaya, B. Joseph, Chem. Eur. J 27, 2299 (2021)
- 32. I.D. Sahu, R.M. McCarrick, K.R. Troxel, R. Zhang, H.J. Smith, M.M. Dunagan, M.S. Swartz, P.V. Rajan, B.M. Kroncke, C.R. Sanders, G.A. Lorigan, Biochemistry **52**, 6627 (2013)
- M.N. Kinde, Q. Chen, M.J. Lawless, D.D. Mowrey, J. Xu, S. Saxena, Y. Xu, P. Tang, Structure 23, 995 (2015)
- C. Pliotas, R. Ward, E. Branigan, A. Rasmussen, G. Hagelueken, H. Huang, S.S. Black, I.R. Booth,
   O. Schiemann, J.H. Naismith, Proc. Natl. Acad. Sci. USA 109, E2675 (2012)
- 35. S. Kucher, C. Elsner, M. Safonova, S. Maffini, E. Bordignon, J. Phys. Chem. Lett. 12, 3679 (2021)
- 36. P. Widder, J. Schuck, D. Summerer, M. Drescher, Phys. Chem. Chem. Phys. 22, 4875 (2020)
- Y. Yang, S.-N. Chen, F. Yang, X.-Y. Li, A. Feintuch, X.-C. Su, D. Goldfarb, Proc. Natl. Acad. Sci. USA 117, 20566 (2020)
- 38. G. Karthikeyan, A. Bonucci, G. Casano, G. Gerbaud, S. Abel, V. Thomé, L. Kodjabachian, A. Magalon, B. Guigliarelli, V. Belle, O. Ouari, E. Mileo, Angew. Chem. Int. Ed. **57**, 1366 (2018)
- R. Igarashi, T. Sakai, H. Hara, T. Tenno, T. Tanaka, H. Tochio, M. Shirakawa, J. Am. Chem. Soc. 132, 8228 (2010)
- 40. K. Singewald, M.J. Lawless, S. Saxena, J. Magn. Reson. **299**, 21 (2019)



- S. Jana, E.G.B. Evans, H.S. Jang, S. Zhang, H. Zhang, A. Rajca, S.E. Gordon, W.N. Zagotta, S. Stoll, R.A. Mehl, J. Am. Chem. Soc. 27, 14608–14620 (2023)
- 42. N. Fleck, C.A. Heubach, T. Hett, F.R. Haege, P.P. Bawol, H. Baltruschat, O. Schiemann, Angew. Chem. Int. Ed. **59**, 9767 (2020)
- O. Schiemann, C.A. Heubach, D. Abdullin, K. Ackermann, M. Azarkh, E.G. Bagryanskaya, M. Drescher, B. Endeward, J.H. Freed, L. Galazzo, D. Goldfarb, T. Hett, L. Esteban Hofer, L. Fábregas Ibáñez, E.J. Hustedt, S. Kucher, I. Kuprov, J.E. Lovett, A. Meyer, S. Ruthstein, S. Saxena, S. Stoll, C.R. Timmel, M. Di Valentin, H.S. Mchaourab, T.F. Prisner, B.E. Bode, E. Bordignon, M. Bennati, G. Jeschke, J. Am. Chem. Soc. 143, 17875 (2021)
- J.L. Sarver, J.E. Townsend, G. Rajapakse, L. Jen-Jacobson, S. Saxena, J. Phys. Chem. B 116, 4024 (2012)
- 45. K. Sale, L. Song, Y.-S. Liu, E. Perozo, P. Fajer, J. Am. Chem. Soc. 127, 9334 (2005)
- 46. A. Gamble Jarvi, X. Bogetti, K. Singewald, S. Ghosh, S. Saxena, Acc. Chem. Res. 54, 1481 (2021)
- 47. A.J. Fielding, M.G. Concilio, G. Heaven, M.A. Hollas, Molecules 19, 16998 (2014)
- 48. W.L. Hubbell, C. Altenbach, Curr. Opin. Struct. Biol. 4, 566 (1994)
- T.F. Cunningham, M.R. Putterman, A. Desai, W.S. Horne, S. Saxena, Angew. Chem. Int. Ed. Engl. 127, 6428 (2015)
- T.F. Cunningham, M.R. Putterman, A. Desai, W.S. Horne, S. Saxena, Angew. Chem. Int. Ed. 54, 6330 (2015)
- 51. H. Ghimire, R.M. McCarrick, D.E. Budil, G.A. Lorigan, Biochemistry 48, 5782 (2009)
- J.L. Wort, K. Ackermann, A. Giannoulis, A.J. Stewart, D.G. Norman, B.E. Bode, Angew. Chem. Int. Ed. 58, 11681 (2019)
- 53. N. Fleck, C. Heubach, T. Hett, S. Spicher, S. Grimme, O. Schiemann, Chem. Eur. J 27, 5292 (2021)
- 54. I. Tkach, G. Sicoli, C. Höbartner, M. Bennati, J. Magn. Reson. 209, 341 (2011)
- D. Akhmetzyanov, P. Schöps, A. Marko, N.C. Kunjir, S.T. Sigurdsson, T.F. Prisner, Phys. Chem. Chem. Phys. 17, 24446 (2015)
- A. Potapov, H. Yagi, T. Huber, S. Jergic, N.E. Dixon, G. Otting, D. Goldfarb, J. Am. Chem. Soc. 132, 9040 (2010)
- G.W. Reginsson, R.I. Hunter, P.A.S. Cruickshank, D.R. Bolton, S.T. Sigurdsson, G.M. Smith, O. Schiemann, J. Magn. Reson. 216, 175 (2012)
- C.L. Motion, J.E. Lovett, S. Bell, S.L. Cassidy, P.A.S. Cruickshank, D.R. Bolton, R.I. Hunter, H. El Mkami, S. Van Doorslaer, G.M. Smith, J. Phys. Chem. Lett. 7, 1411 (2016)
- 59. M.H. Tessmer, S. Stoll, PLoS Comput. Biol. 19, e1010834 (2023)
- 60. X. Bogetti, S. Ghosh, A. Gamble Jarvi, J. Wang, S. Saxena, J. Phys. Chem. B 124, 2788 (2020)
- P.E. Spindler, Y. Zhang, B. Endeward, N. Gershernzon, T.E. Skinner, S.J. Glaser, T.F. Prisner, J. Magn. Reson. 218, 49 (2012)
- F.D. Breitgoff, K. Keller, M. Qi, D. Klose, M. Yulikov, A. Godt, G. Jeschke, J. Magn. Reson. 308, 106560 (2019)
- 63. A. Doll, G. Jeschke, J. Magn. Reson. 246, 18 (2014)
- 64. I. Kaminker, R. Barnes, S. Han, J. Magn. Reson. 279, 81 (2017)
- 65. V. Denysenkov, P. van Os, T.F. Prisner, Appl Magn Reson 48, 1263 (2017)
- 66. J.W. Sidabras, T. Sarna, R.R. Mett, J.S. Hyde, J. Magn. Reson. 282, 129 (2017)
- 67. M. Ji, S. Ruthstein, S. Saxena, Acc. Chem. Res. 47, 688 (2014)
- C.M. Grytz, A. Marko, P. Cekan, S.T. Sigurdsson, T.F. Prisner, Phys. Chem. Chem. Phys. 18, 2993 (2016)
- 69. A. Godt, M. Schulte, H. Zimmermann, G. Jeschke, Angew. Chem. Int. Ed. 45, 7560 (2006)
- 70. T.F. Prisner, A. Marko, S.T. Sigurdsson, J. Magn. Reson. 252, 187 (2015)
- A.M. Bowen, A. Bertran, K.B. Henbest, M. Gobbo, C.R. Timmel, M. Di Valentin, J. Phys. Chem. Lett. 12, 3819 (2021)
- I. Kaminker, I. Tkach, N. Manukovsky, T. Huber, H. Yagi, G. Otting, M. Bennati, D. Goldfarb, J. Magn. Reson. 227, 66 (2013)
- A. Gamble Jarvi, K. Ranguelova, S. Ghosh, R.T. Weber, S. Saxena, J. Phys. Chem. B 122, 10669 (2018)
- V.P. Denysenkov, T.F. Prisner, J. Stubbe, M. Bennati, Proc. Natl. Acad. Sci. USA 103, 13386 (2006)
- 75. Z. Yang, D. Kise, S. Saxena, J. Phys. Chem. B **114**, 6165 (2010)
- 76. D. Abdullin, G. Hagelueken, R.I. Hunter, G.M. Smith, O. Schiemann, Mol. Phys. 113, 544 (2015)
- 77. A. Marko, T.F. Prisner, Phys. Chem. Chem. Phys. 15, 619 (2013)



- 78. A. Potapov, J. Magn. Reson. **316**, 106769 (2020)
- 79. A.G. Maryasov, Y.D. Tsvetkov, J. Raap, Appl. Magn. Reson. 14, 101 (1998)
- 80. Z. Hasanbasri, N.A. Moriglioni, S. Saxena, Phys. Chem. Chem. Phys. 25(19), 13275-13288 (2023)
- 81. X. Bogetti, Z. Hasanbasri, H.R. Hunter, S. Saxena, Phys. Chem. Chem. Phys. 24, 14727 (2022)
- 82. P. Roser, M.J. Schmidt, M. Drescher, D. Summerer, Org. Biomol. Chem. 14, 5468 (2016)
- 83. D. Goldfarb, Phys. Chem. Chem. Phys. 16, 9685 (2014)
- 84. S. Jun, J.S. Becker, M. Yonkunas, R. Coalson, S. Saxena, Biochemistry 45, 11666 (2006)
- 85. Z. Yang, J. Becker, S. Saxena, J. Magn. Reson. 188, 337 (2007)
- T.F. Cunningham, M.D. Shannon, M.R. Putterman, R.J. Arachchige, I. Sengupta, M. Gao, C.P. Jaroniec, S. Saxena, J. Phys. Chem. B 119, 2839 (2015)
- 87. S. Ghosh, M.J. Lawless, H.J. Brubaker, K. Singewald, M.R. Kurpiewski, L. Jen-Jacobson, S. Saxena, Nucleic Acids Res. 48, e49 (2020)
- 88. Y. Polyhach, A. Godt, C. Bauer, G. Jeschke, J. Magn. Reson. 185, 118 (2007)
- A. Gamble Jarvi, A. Sargun, X. Bogetti, J. Wang, C. Achim, S. Saxena, J. Phys. Chem. B 124, 7544 (2020)
- 90. S. Ghosh, M.J. Lawless, G.S. Rule, S. Saxena, J. Magn. Reson. **286**, 163 (2018)
- M.J. Lawless, S. Ghosh, T.F. Cunningham, A. Shimshi, S. Saxena, Phys. Chem. Chem. Phys. 19, 20959 (2017)
- 92. K. Singewald, J.A. Wilkinson, A.S. Saxena, Bio Protoc 11, e4258 (2021)
- 93. W. R. Hagen, Biomolecular EPR Spectroscopy (CRC Press, 2008)
- 94. K. Singewald, X. Bogetti, K. Sinha, G.S. Rule, S. Saxena, Angew. Chem. Int. Ed. 59, 23040 (2020)
- 95. A. Gamble Jarvi, J. Casto, S. Saxena, J. Magn. Reson. 320, 106848 (2020)
- S. Stoller, G. Sicoli, T.Y. Baranova, M. Bennati, U. Diederichsen, Angew. Chem. Int. Ed. 50, 9743 (2011)
- 97. K. Halbmair, J. Wegner, U. Diederichsen, M. Bennati, Biophys. J. 111, 2345 (2016)
- 98. M.R. Fleissner, M.D. Bridges, E.K. Brooks, D. Cascio, T. Kálai, K. Hideg, W.L. Hubbell, Proc. Natl. Acad. Sci. USA 108, 16241 (2011)
- 99. M.A. Stevens, J.E. McKay, J.L.S. Robinson, H. El Mkami, G.M. Smith, D.G. Norman, Phys. Chem. Chem. Phys. 18, 5799 (2016)
- H. Sameach, S. Ghosh, L. Gevorkyan-Airapetov, S. Saxena, S. Ruthstein, Angew. Chem. Int. Ed. 58, 3053 (2019)
- 101. B.G. Dzikovski, P.P. Borbat, J.H. Freed, J. Phys. Chem. B 115, 176 (2011)
- 102. B. Endeward, J.A. Butterwick, R. MacKinnon, T.F. Prisner, J. Am. Chem. Soc. 131, 15246 (2009)
- M.V. Fedin, G.Y. Shevelev, D.V. Pyshnyi, V.M. Tormyshev, G. Jeschke, M. Yulikov, E.G. Bagryanskaya, Phys. Chem. Chem. Phys. 18, 29549 (2016)
- 104. D. Abdullin, G. Hagelueken, O. Schiemann, Phys. Chem. Chem. Phys. 18, 10428 (2016)
- 105. P. Cekan, E.O. Jonsson, S.T. Sigurdsson, Nucleic Acids Res. 37, 3990 (2009)
- M. Heinz, N. Erlenbach, L.S. Stelzl, G. Thierolf, N.R. Kamble, S.T. Sigurdsson, T.F. Prisner, G. Hummer, Nucleic Acids Res. 48, 924 (2020)
- L.S. Stelzl, N. Erlenbach, M. Heinz, T.F. Prisner, G. Hummer, J. Am. Chem. Soc. 139, 11674 (2017)
- D.M. Engelhard, A. Meyer, A. Berndhäuser, O. Schiemann, G.H. Clever, Chem. Commun. 54, 7455 (2018)
- L.M. Stratmann, Y. Kutin, M. Kasanmascheff, G.H. Clever, Angew. Chem. Int. Ed. 60, 4939 (2021)
- 110. M.P. Donohue, V.A. Szalai, Phys. Chem. Chem. Phys. 18, 15447 (2016)
- C.M. Grytz, S. Kazemi, A. Marko, P. Cekan, P. Güntert, S.T. Sigurdsson, T.F. Prisner, Phys. Chem. Chem. Phys. 19, 29801 (2017)
- G.W. Reginsson, S.A. Shelke, C. Rouillon, M.F. White, S.T. Sigurdsson, O. Schiemann, Nucleic Acids Res. 41, e11 (2013)
- 113. S. Stoll, A. Schweiger, J. Magn. Reson. 178, 42 (2006)
- 114. D. Abdullin, Appl Magn Reson **51**, 725 (2020)
- 115. A.M. Bowen, M.W. Jones, J.E. Lovett, T.G. Gaule, M.J. McPherson, J.R. Dilworth, C.R. Timmel, J.R. Harmer, Phys. Chem. Chem. Phys. 18, 5981 (2016)
- J.E. Lovett, A.M. Bowen, C.R. Timmel, M.W. Jones, J.R. Dilworth, D. Caprotti, S.G. Bell, L.L. Wong, J. Harmer, Phys. Chem. Chem. Phys. 11, 6840 (2009)
- 117. D. Margraf, B.E. Bode, A. Marko, O. Schiemann, T.F. Prisner, Mol. Phys. 105, 2153 (2007)



- C. Abé, D. Klose, F. Dietrich, W.H. Ziegler, Y. Polyhach, G. Jeschke, H.-J. Steinhoff, J. Magn. Reson. 216, 53 (2012)
- 119. A. Savitsky, A.A. Dubinskii, M. Flores, W. Lubitz, K. Möbius, J. Phys. Chem. B 111, 6245 (2007)
- A.M. Bowen, E.O.D. Johnson, F. Mercuri, N.J. Hoskins, R. Qiao, J.S.O. McCullagh, J.E. Lovett,
   S.G. Bell, W. Zhou, C.R. Timmel, L.L. Wong, J.R. Harmer, J. Am. Chem. Soc. 140, 2514 (2018)
- 121. A. Marko, D. Margraf, H. Yu, Y. Mu, G. Stock, T. Prisner, J. Chem. Phys. 130, 064102 (2009)
- 122. G. Jeschke, V. Chechik, P. Ionita, A. Godt, H. Zimmermann, J. Banham, C.R. Timmel, D. Hilger, H. Jung, Appl Magn Reson 30, 473 (2006)
- A. Giannoulis, C.L. Motion, M. Oranges, M. Bühl, G.M. Smith, B.E. Bode, Phys. Chem. Chem. Phys. 20, 2151 (2018)
- 124. A. Meyer, D. Abdullin, G. Schnakenburg, O. Schiemann, Phys. Chem. Chem. Phys. 18, 9262 (2016)
- D. Abdullin, P. Brehm, N. Fleck, S. Spicher, S. Grimme, O. Schiemann, Chem. Eur. J 25, 14388 (2019)
- 126. H.L. Flanagan, G.J. Gerfen, A. Lai, D.J. Singel, J. Chem. Phys. 88, 2162 (1988)
- 127. G.H. Rist, J.S. Hyde, J. Chem. Phys. 52, 4633 (1970)
- A. Kehl, M. Hiller, F. Hecker, I. Tkach, S. Dechert, M. Bennati, A. Meyer, J. Magn. Reson. 333, 107091 (2021)
- 129. G.E. Cutsail, J. Telser, B.M. Hoffman, Biochim. Biophys. Acta 1853, 1370 (2015)
- R. Kappl, G. Bracic, J. Hüttermann, in *High Resolution EPR*. ed. by L. Berliner, G. Hanson (Springer, New York, New York, NY, 2009), pp.63–103
- T. Iwasaki, A. Kounosu, T. Uzawa, R.I. Samoilova, S.A. Dikanov, J. Am. Chem. Soc. 126, 13902 (2004)
- N. Wili, S. Richert, B. Limburg, S.J. Clarke, H.L. Anderson, C.R. Timmel, G. Jeschke, Phys. Chem. Chem. Phys. 21, 11676 (2019)

**Publisher's Note** Springer Nature remains neutral with regard to jurisdictional claims in published maps and institutional affiliations.

Springer Nature or its licensor (e.g. a society or other partner) holds exclusive rights to this article under a publishing agreement with the author(s) or other rightsholder(s); author self-archiving of the accepted manuscript version of this article is solely governed by the terms of such publishing agreement and applicable law.

